DENSE GAS PLUME RISE AND TOUCHDOWN FOR JACK RABBIT II TRIAL 8 CHLORINE FIELD EXPERIMENT

Steven Hanna[1], Graham Tickle[2], Thomas Mazzola[3], and Simon Gant[4]

[1]Hanna Consultants, Kennebunkport, ME, USA; [2]GT Science and Software, UK; [3]SAIC, Lorton, VA, USA, [4] HSE, UK

Abstract: The series of nine Jack Rabbit II (JR II) chlorine release field experiments in 2015 and 2016 involved releases of pressurized liquefied chlorine from tanks containing 5 to 20 tons of liquid. This paper concerns JR II Trial 8, where the release hole (15.2 cm diameter) was oriented upwards at the top of the tank. To our knowledge, this is the only full-scale vertically-directed release of pressurized liquefied chlorine that is available for detailed analysis. Our aim is to improve understanding of the characteristics of the dense jet trajectory (e.g., maximum plume rise, downwind distance where the dense plume first touches the ground, and maximum concentration at touchdown). The chlorine emission rate was measured by instruments in the tank, and the plume rise geometry was estimated from photographs, videos, and lidar scans taken from several angles. During the first 10 seconds of the release, the videos show that the dense jet rises up to about 40 m, then sinks towards the ground, touching down at a distance of about 60 m. The portion of the plume that sinks to the ground then spreads out about 30 to 40 m in all directions due to gravity slumping. Due to the decrease with time of the momentum jet mass release rate, the jet gradually becomes less dense and less powerful and the plume remains aloft after about 30 to 60 s. However, the dense cloud that touched down in the early phases moves downwind as a typical dense cloud. The observed dense jet plume rise and touchdown distance are shown to approximately agree within about a factor of two with integral model predictions by 1) the analytical dense gas plume formulas suggested for vertical jets in 1973 by Hoot, Meroney, and Peterka (HMP), 2) the analytical formula for buoyant (positive or negative) plume trajectory suggested by Briggs in 1969, and 3) the DRIFT dispersion software, which is an integral model. Also, HMP and DRIFT model predictions of concentration at touchdown agree with Trial 8 observations within a factor of about two. It is concluded that the dense jet plume models are able to simulate the Trial 8 plume trajectory and ground level maximum concentration within acceptable ranges (i.e., most of time, within a factor of two).

Key words: *dense gas dispersion; chlorine releases; plume rise of dense jet; touchdown of dense jet plume, Jack Rabbit II field study*

INTRODUCTION

The Jack Rabbit field experiments in 2010, 2015, and 2016 were initiated because there had been much concern about the possible effects of pressurized liquid chlorine released from storage tanks and transportation vessels. The JR I field experiments, which took place at Dugway Proving Ground (DPG) in the U.S. in 2010, addressed one and two ton releases of pressurized liquefied chlorine or ammonia from a tank mounted about 1 m above ground, with the initial jet pointed downward (Fox and Storwold 2010, Bauer 2013, Hanna et al. 2012 and 2016). JR II took place in 2015 and 2016, also at DPG, and involved nine chlorine release trials, with released amounts of about 5 to 20 tons (Fox et al., 2021).

A special virtual issue of this journal (in which the current manuscript is placed) contains papers related to a 17-model comparison exercise that used observations from JR II trials 1, 6, and 7, which all involved downward-directed jets. Several of the special issue papers are general (i.e., apply to all nine trials), covering topics such as a comprehensive project overview (Fox et al., 2021), a discussion of source emissions (Spicer and Tickle, 2020), recommendations on meteorological inputs (Hanna, 2020), a description of concentration observations (Chang et al, 2020), and a summary of the results of the 17-model comparison study (Mazzola et al., 2020). Because these general papers are available, we will refer the reader to those papers for comprehensive discussions of some topics.

The current paper analyzes the dense gas plume observed during JR II Trial 8, the only trial with an upward directed release. Trial 8 received only limited attention in the multi-model comparison, which focused on downwards-directed releases. The main novelty is that JR Trial 8 is the only extensively controlled and measured full-scale field trial in existence involving pressure-liquefied chlorine where the discharge is upwards from the top of the vessel. The outflow exhibits complex behavior with a very short (one or two seconds) duration initial gas venting stage, followed by about 30 s of two-phase venting (due to liquid swell within the vessel – the champagne effect), through to the final stage of gas-phase venting, which approached negligible discharge rate at about 100 s. Several models that are commonly used for industrial risk assessments do not account for this complex physics, and, instead, would simulate Trial 8 as a purely gaseous release (as a consequence, it is likely that such models would under-predict the hazard at ground level). There are therefore important practical reasons to study this experiment, since it provides risk assessment specialists and emergency responders with some insight into what would happen in this release scenario. It also provides useful scientific data that can be used to assess the accuracy of dispersion models. Models have not been tested against the Trial 8 observations previously. It is therefore useful to disseminate in the scientific literature the data from this unique experiment to enable others to test their models against the measurements. Plus, we have examined the performance of three integral dispersion models against the data.

Our aim is not to describe the experimental set-up in significant detail, since, as mentioned above, there are already published papers in the special issue that describe the JR II details. Because this is the only available field data set for large upwards-directed dense jets, it is of initial interest to determine whether the dense jet plume trajectory and maximum ground level concentration are consistent with the physical principles assumed by integral dispersion models. The models solve for the variation with downwind distance of the cross-wind integral of concentration, which is described by a simple shape function. For the Briggs (1969) and the Hoot-Meroney-Peterka (HMP, 1973) models, the cross-wind shape is a top hat. For DRIFT (Tickle and Carlisle 2013), the cross-wind distribution is a Gaussian profile (for the momentum-jet phase). Integral models are routinely used when assessing hazards for regulatory and safety purposes. It is therefore of practical interest to compare the observed plume behavior in Trial 8 with predictions from this class of models. A benefit of integral

dispersion models, as well as their execution speed, is that they provide insights into the dominant physics controlling the bulk behavior of the plume.

The three dense gas plume models for vertical releases that we use here are based on early seminal studies of dense gas plumes by Bodurtha (1961) and Turner (1966). Bodurtha (1961) carried out wind tunnel tests with dense plumes and focused on determining how far from the source the dense cloud touched the ground, and the magnitude of the maximum ground level concentration. Empirical formulas were suggested. Turner (1966) focused more on analytical solutions to the fundamental governing equations. Briggs (1969) looked at a large amount of plume rise literature, for both positive and negative buoyant plumes, developed a set of universal dimensionless equations based on fundamental science, and used available laboratory and field date to determine the scaling constants in his equations. His suggested plume rise trajectory formula is used in the current paper.

Hoot et al. (1973) and Hoot and Meroney (1974) carried out a new set of wind tunnel experiments for vertically-oriented dense jets. Building on Briggs' (1969) approach, they developed some simple science based analytical formulas that produced good fits to their observations. We use those formulas here.

At about the same time as the Hoot et al. experiments, Ooms and his colleagues began a comprehensive theoretical analysis of dense jets and carried out a series of wind tunnel experiments (Ooms et al. 1974, Ooms and Duijm 1984, Xiao-Yun et al. 1985). Cleaver and Edwards (1990) suggest an alternate dense gas jet model and compare it with experimental data. A few years later, Schatzmann et al. (1995a and 1995b) report results of EPA wind tunnel experiments involving heavy gas jets and used the data to calibrate and further test a dense jet model. The above wind tunnel experiments verified the accuracy of the investigators' models.

Other more recent papers (e.g., Allason et al., 2014) include dense gas jets as one component of a more comprehensive research study. They carried out small-scale experiments with dense jets "outdoors" and compared the results with the predictions of the Cleaver and Edwards (1990) model.

In the above papers on dense gas vertical jets, the photographs and figures all show a similar behavior, with the dense jet initially rising quickly to a maximum plume rise, followed by a more gradual descent to the ground. Of course, if the initial negative buoyancy is not large enough, the plume will not sink down to the ground. This too is accounted for by the models. When we sent Dr. Robert Meroney (coauthor of the 1973 HMP model) the photographs of the JR II Trial 8 plume, he remarked in a 6 March 2021 e-mail message: "This photo looks remarkably like the dense gas plumes Tom Hoot visualized in our wind tunnel. The arc and spread of the plume, the impact with the ground, and the pancake-like spreading up and downstream after the impact. We tried to document the height of rise, the impact location, and the maximum concentration at impact, as well as the subsequent down and upwind decay of the ground concentrations".

To compare the three models' predictions with the JR Trial 8 observations, a challenge arises with two-phase releases that is not present in the wind tunnel and the small-scale outdoors experiments reviewed above. The difficulty is that the dense two-phase jet exiting the hole on the Trial 8 tank has a pressure that is several times larger than atmospheric pressure. However, it is common for models to require initial inputs of plume volume flux, radius, vertical velocity, and density to be at atmospheric pressure. Therefore, an "expansion model" is needed to calculate the initial conditions for the models. Fortunately, for Trial 8, the pressure in the jet decreases to atmospheric pressure within about 2 to 3 m of travel, which is much less than the observed plume rise of about 40 m and observed touchdown distance of about 50 m. Here, we use two alternate widely-used expansion models to define the initial inputs to the models.

OVERVIEW OF JR II TRIAL 8

The nine JR II field trials took place over an extensive dry lake bed (salt playa) with minimal vegetation at DPG, where the surface roughness was determined to be about 0.5 mm (Fox et al., 2021). The release was initiated between about 7 to 9 AM (depending on when the wind speed and direction were within prescribed bounds) in late August and early September of both 2015 and 2016. The release tank containing pressure liquefied chlorine was at the center of a 25 m diameter concrete pad. Identical 15.2 cm (6.0 inch) holes were located at the bottom, the top, and at a 45 degree downwards angle on a horizontal ten-ton tank (Nicholson et al. 2017 and Spicer and Miller 2018). The bottom of the tank was located 1 m above ground level (agl) and the tank was 1.37 m (54 inches) in diameter. The hole was at the top of the tank for Trial 8, as identified in Figure 1. The Trial 8 release on 11 September 2016 began at 9:01:45 am Mountain Daylight Time (LDT); or 15:01:45 GMT. The initial chlorine mass in the tank was 9100 kg, the release duration (two phase jet phase) was about 30 s and total mass released in the jet was 2400 kg.

Figure 1. Photo of JR II ten ton release tank. The arrow depicts the upward jet release location at the top of the tank used in Trial 8. The bottom of the tank is 1 m above ground level.

The observed air temperature was 15.8 °C and estimated air density was 1.05 kg m^{-3}. Winds were observed by a network of about 35 portable 2 m towers, supplemented by three 32 m towers with sonic anemometers at heights of 2, 4, 8, 16, and 32 m; one of the towers was less than 100 m upwind of the JR II release tank. For the 10-minute period after the release, wind speed at a height of 2 m near the source location was 2.1 m s^{-1}, and wind direction was from 120° (Hanna, 2020). Wind speed increased to 2.9 m s^{-1} at z = 16 m and 3.9 m s^{-1} at z = 100 m. Wind direction veered to about 165° between z = 32 and 100 m. Over the next 20 minutes, the surface wind direction near the source slowly veered to about 155° and the mean 10 minute averaged wind speed at 2 m first increased to 2.9 m s^{-1} and then decreased to about 1.5 m s^{-1}.

As is typical in the early morning, the boundary layer stability varied significantly in time and space. A deep (hundreds of meters) stable layer had formed during the night (see plots of temperature profiles in Hanna, 2020) and persisted in the early morning. For example, temperatures at 100 m were about 2 or 3 °C higher than at the surface at the time of the release. However, the morning sun had warmed the surface enough that a weak upward sensible heat flux was observed by sonic anemometers at 2 m, and a shallow (4 to 8 m) unstable layer had formed. Above the 8 m level, the boundary layer remained slightly stable. Thus, the boundary layer is not steady-state, and standard Monin-Obukhov formulas for wind and temperature and turbulence profiles are not strictly applicable. Also, the so-called "mixing depth" is not well-defined.

As was done for all nine JR II trials, concentrations (at 0.3 m) and winds (at 2 m) were measured at all directions around the circle for downwind distances of about 50 to 120 m, and on 90° arcs at distances of 0.2, 0.5, 1, 2, 5, and 11 km (see Chang et al., 2021). The 360° coverage in the near field was intended to capture the gravity slumping in all directions, which extended about 50 to 100 m in most trials. The 90° arcs were centered on the expected dominant wind direction (from 165°).

Still photos and videos were taken by cameras located at several near-ground sites to the side of the expected cloud direction and from the rear. These were essential for estimating the maximum plume rise and touchdown distance for the plume in Trial 8. In addition, a drone, operated by Utah Valley University, was used to take videos from above the chlorine cloud. Since the hole was at the top of the tank during Trial 8, over 70 % of the chlorine liquid remained in the tank after the momentum jet decreased to nearly zero after about 100 s. This remaining liquid was "dumped" onto the concrete pad about 10 minutes later and subsequently evaporated over 10 to 20 minutes. Chlorine samplers continued to collect data during this period, thus effectively creating an additional "trial" that could be used to test evaporating pool models. The current paper deals only with the jet release component, not the subsequent liquid dump.

Fox et al. (2021) and Mazzola et al. (2021) include tables of basic characteristics (e.g., mass released, start time, duration, wind speed and direction, ambient temperature and a measure of stability) of the releases for all JR II trials. Here, though, we include additional details for Trial 8, such as the variation of mass emission rate with time, and

we calculate the initial conditions needed for input to the models. As mentioned at the end of the previous section, the conditions at the exit hole could not be used as initial conditions because the effluent is overpressured at the hole. We use two alternate expansion models to estimate the initial cloud density, vertical velocity, and radius at the point (about 2 m from the hole) where the pressure drops almost to ambient.

OBSERVATIONS OF DENSE JET RISE IN TRIAL 8

Spicer and Miller (2018) and Spicer and Tickle (2020) used observations inside the tank to explain that the vapor release during Trial 8 lasted only one or two seconds, followed by a two-phase jet that lasted about 30 s. This was followed by a steadily diminishing gas jet for another 60 or 70 s. The videos from the side showed a brief initial yellow-green vapor cloud, followed by a white two-phase cloud in the rise phase until about 25 to 30 s after the release started. After the plume centerline rose to a height of about 40 m at a distance of about 20 m downwind, the plume's excess density caused it to sink to the ground, reaching the ground at a downwind distance of about 50 m. The sinking yellow-green cloud appeared to be gas phase only (without aerosol droplets) as it was approaching the ground. The videos indicated that, over a period of about 30 s, the plume "touchdown" distance increased from about 50 m initially to about 100 m. After that, due the decrease in density of the plume, the visible green plume remained aloft.

The observations that we use in the analysis of the dense jet are mostly based on scaling of photographs. There were no in situ measurements in the chlorine plume aloft. As discussed by Chang et al. (2021), the only in situ concentration measurements within 100 m of the source were at near-ground sensors in the closest 100 m from the source. Those measurements were used to test the models' predictions of maximum ground level concentration at ground level at the distance of plume touchdown. The available observations for determining the plume trajectory aloft were still photographs and videos, and limited lidar data. The photos and videos were taken by high quality cameras set up at several locations by Dugway Proving Ground. The lidar observations were scans of the plume taken from a distance of about 1.5 km, on either side of the plume (Ponsardin, 2017). Because the lidar could not penetrate very far into the plume, only the edges of the plume could be seen.

Measured distances from the images (still and video) were obtained by setting a distance scale based on the known height of the camera scaffold towers (21 ft = 6.4m) shown in Figure 2 (with arrows drawn to show the measurements taken from these particular image frames). For the horizontal distances, a small correction has been included to account for the fact that the plume axis is not aligned exactly perpendicular to the camera line of view. The plume axis direction was estimated from overhead drone video footage.

The plume centerline location was estimated visually by following the plume path on the video frames. The measurements of distances from the frames were made using freely available software, which sets a scale on an image and takes further

measurements with that scaling applied. The main uncertainty was in judging the centerline of a sometimes-billowing plume structure. Our estimates of these distances have an uncertainty of approximately 20% in the horizontal and vertical distances to the maximum plume centerline height, and a larger uncertainty of approximately 30% in the horizontal distance at which the center of the plume touches down. The touchdown uncertainty is larger due to the visual complexity caused by gravity induced spreading of the grounded portion of the cloud.

Although these methods of determining the centerline from analysis of photographs and videos may seem approximate, it is judged sufficiently accurate for the present purposes. Commonly, when dispersion models are compared to data from large-scale field trials, they are judged to be acceptable if the errors are less than a factor of two.

Figure 2 contains a time sequence of photos of the Trial 8 plume, illustrating how the plume maximum rise, the distance to maximum rise, and the distance to touchdown were estimated. The camera towers used for distance scaling are indicated. There are five panels, showing the plume from the side, for times after release of 6, 12, 20, 28, and 35 s. These times were chosen to show the progression of the visible plume behavior. It is important to recognize that the observed plume at a distance of 100 m downwind in a photo represents the chlorine that was released about 30 seconds earlier, since the cloud is travelling downwind at approximately the speed of the wind (2 to 3 m s^{-1}). In the near field, the high-velocity jet rapidly projects the chlorine upwards, which is then transported by the wind and simultaneously entrains ambient air. Times of 12 and 20 s are included in Figure 2 because the videos suggest that the first plume "touchdown" occurred during that time period after release. After touchdown, the ground-based cloud seen in the photos at 28 and 35 s spreads out about 30 or 40 m in all directions, and is advected downwind by the ambient wind.

Videos and photos were also analyzed for times after release exceeding 100 s. However, at those larger times, two different clouds are seen – One hugging the ground and containing plume material that touched down during the first 30 or 40 s after the release, and another at an elevation of about 30 to 50 m resulting from chlorine gas released after 30 or 40 s, that remained aloft (i.e., did not sink to the ground)

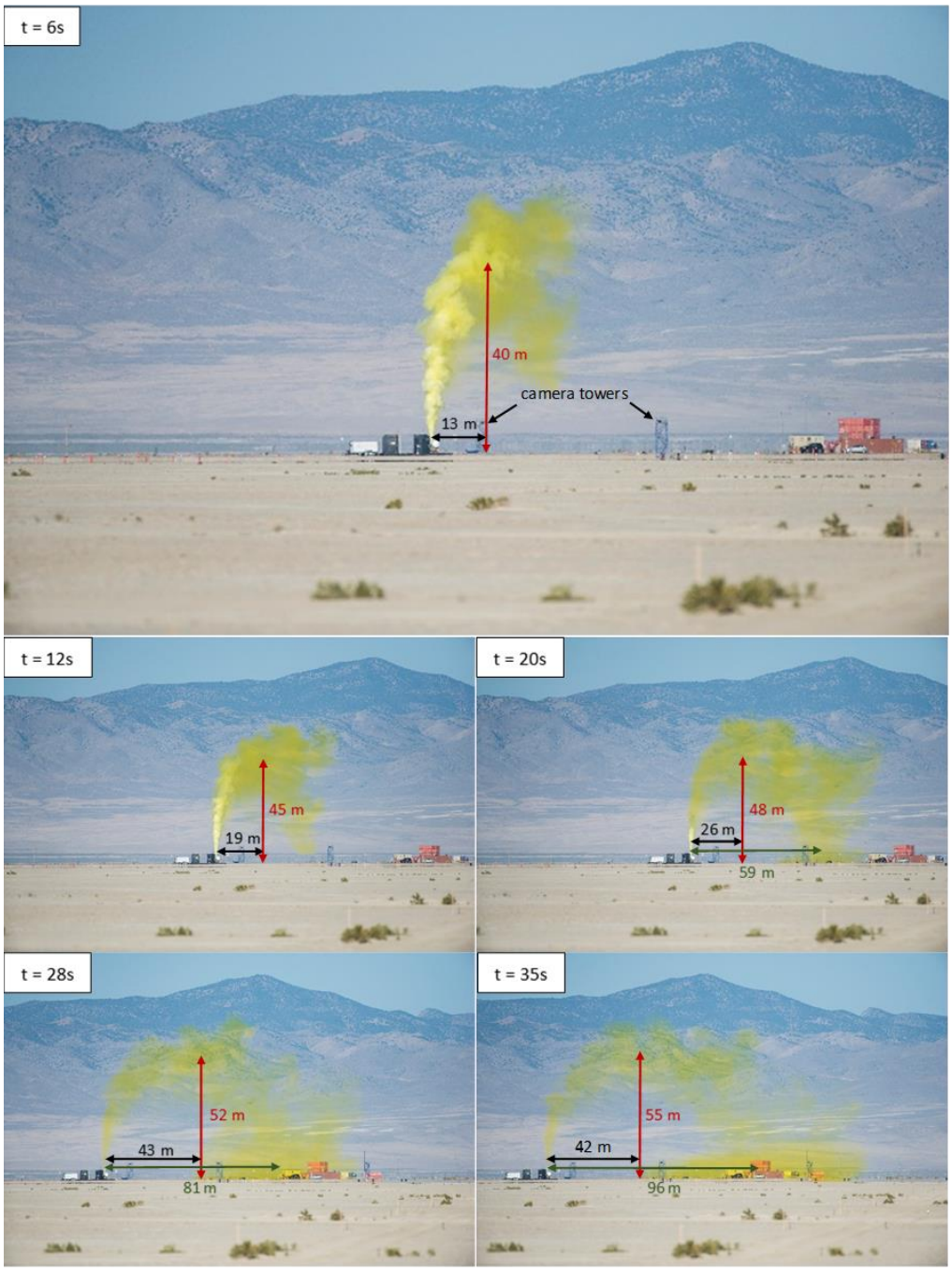

Figure 2. Sequence of still images of Trial 8. Times are seconds after the release was initiated and are approximate, having been estimated from the times indicated on videos. The camera towers used for setting the vertical length scale are indicated on the first image. The estimated maximum plume height, distance to maximum plume height, and distance to touchdown are indicated. The portion of the plume with a whitish tinge is where there are two phases (i.e., aerosols imbedded).

The maximum centerline rise height increased from approximately 40 m at 10 s to approximately 60 m at 40 s. Similarly, the horizontal distance to the maximum plume rise increased from approximately 20 m at 10 s to approximately 50 m at 40 s. Over this time period, the emission was two-phase and the emission mass flux, emission momentum flux and the emission density decreased by large factors. However, the emission velocity increased due to the increased vapor fraction over time. These are competing effects that could have different effects on the plume behavior. Increasing the vertical velocity and decreasing the density would be expected to increase the plume rise, whereas reducing the mass flux would be expected to diminish the plume rise. The observed trajectory behavior suggests that the net effect was to initially increase the rise during the two-phase venting period. After about 60 s, when the vessel was venting only vapor, the maximum rise height was observed to decrease slightly with time, which is consistent with a diminishing emission velocity as the pressure in the vessel decreased.

The observed plume touchdown distance is estimated to be about 50 m at about 10 s and about 100 m at about 40 s. The observed maximum concentration for the jet release in Trial 8 is 12080 ppm at a distance of 85 m (Chang et al., 2021).

As confirmatory evidence of these video and photo observations, Ponsardin (2017) describes lidar observations of the aerosol content of the Trial 8 plume. The two lidars were 1.5 km to the side of the plume. Only the edges of the plume could be seen. The lidar data confirm a first touchdown point for aerosols as 50 m, though somewhat later in time than the vapor plume touchdown from Figure 2. Also, the lidar detected aerosols at heights extend to 42-43 m above ground at times after release of 6-8 s, further confirming the video and photo estimates of maximum plume rise at a time of about 10 s.

As mentioned earlier, the values of observed maximum plume rise and distances to maximum rise and touchdown are based on snapshots at certain times after the release began. However, the part of the cloud that is seen to be touching down on the photo may have been emitted 10 to 40 s earlier. This complicates our comparisons of observations with model predictions, which are produced assuming steady-state conditions and using inputs (e.g., initial density, radius, and vertical velocity) based on 5 or 10 s time increments after release.

It is possible that, when the plume is not sufficiently dense, a horizontal plume (i.e., with approximately constant plume centerline height) may visually appear to "touchdown" by virtue of its bottom edge touching the ground, despite the plume centerline remaining aloft. This does not mean that the plume center has reached ground level. Also, over sufficient travel distance and in the presence of a mixing depth (a cap to upwards dispersion), even in the absence of downward gravitational motion, vertical mixing will result in a nearly constant concentration from ground level to the mixing depth.

When we view the various videos for Trial 8, including a Utah Valley University drone video that was taken from about 100 m above the plume, it appears that the ground-level cloud passes over and around the few obstacles (small trailers and Container Express (CONEX) shipping containers) in its path, even having a clear zone in the wake behind the obstacles. This is consistent with the typical recirculating wake flow around an obstacle, first "piling up" in front of the obstacle, then passing around and over the obstacle. If most of the cloud is at heights less than the obstacle height, there often is a partially clear area of length about 5 or 10 m visible in the wake immediately behind the obstacle. These phenomena are better seen in the videos for the other trials, which had downward-directed releases.

MASS EMISSION RATE AND OTHER SOURCE INPUTS

To calculate the Trial 8 plume trajectory and concentrations at plume touchdown, models require specification of conditions at the location where the jet leaves the storage tank. Some models can treat the complex thermodynamics that occur in the first few meters after the jet passes through the hole, when the jet is depressurizing and approaching ambient pressure. This is often called the expansion zone. However, most dense jet models require that initial conditions be specified assuming that the jet is at ambient pressure. Spicer and Miller (2018) and Spicer and Tickle (2020) have determined these input conditions at ambient pressure for the JR II releases. Based on their analysis of the observed tank conditions during Trial 8, they suggest the mass emission rate variation with time after the release begins, as plotted in Figure 3. Note the constant release rate for the first two seconds (all vapor), the rapid decrease with time (e.g., a factor of about 3 decrease by 10 s), and also the long "tail" where the mass emission rate is slowly decreasing. For the first 1 or 2 s, the release was all-vapor, then switched to two-phase. The presence of liquid aerosols after a few seconds is evident from the visual appearance of the plume – droplets in the plume ke the cloud opaquer and more reflective (white appearance). A chlorine vapor plume appears yellow-green and is not opaque. The observed transition in appearance of the Trial 8 plume is also in good correspondence with the transition predicted by modelling the discharge rate over time (Spicer and Tickle, 2020).

No droplet size measurements are available for this particular release. However, the fraction of the chlorine mass in the initial jet that is in liquid phase will likely consist of very small aerosol drops with a mass mean diameter of about 50 μm (Britter et al., 2011). This size range is expected because the same liquid break-up mechanisms are expected to hold as in flashing releases of other chemicals. After expanding to atmospheric pressure, but before mixing with air, the jet temperature will be close to the chlorine boiling point of -34 °C.

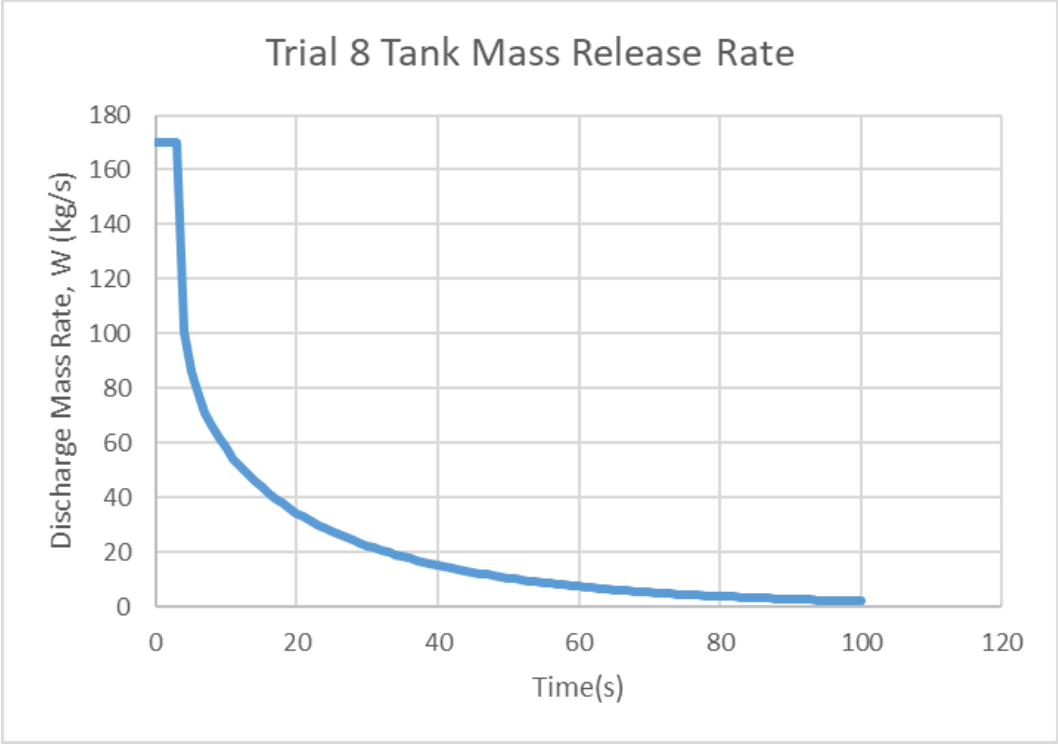

Figure 3. Mass emission rate as a function of time after the release was initiated (from Spicer and Tickle, 2020).

A few models can simulate the plume behavior starting at the hole on the tank, when the jet has a pressure much larger than the ambient pressure. However, as mentioned earlier, most models cannot simulate the plume behavior within the depressurizing jet itself (within about the first 2 or 3 m from the hole in this case), but instead apply pseudo-source conditions once the jet has expanded to reach atmospheric pressure. In our analysis of Trial 8, the initial conditions were defined as a function of time (in piecewise blocks) after the release started, since the mass flux significantly decreased over time.

Spicer and Tickle (2020) discuss methods of estimating plume conditions after depressurization (expansion). Pseudo-source expansion models bridge this expansion zone by making certain simplifying assumptions applied to a control volume. Typical assumptions are that during expansion, heat transfer with surroundings is ignored, mixing with air is ignored, equilibrium is restored between phases. There are alternative assumptions relating to the velocity change on expansion - two alternative approaches are considered for this study:

> Expansion Model 1. Velocity increases above the exit value due to acceleration by excess pressure at the exit. This is also referred to as a momentum conservation model (e.g., Britter et al., 2011)

Expansion Model 2. Velocity unchanged from exit velocity (e.g., Ewan and Moodie, 1986)

Although DRIFT's default modeling (Tickle and Carlisle, 2013) corresponds with Expansion Model 1, both expansion models are tested with DRIFT in the current exercise. Thus, the Expansion Model 1 and Model 2 inputs are used for all three models (HMP, Briggs, and DRIFT). Witlox et al. (2017) found that the conservation of momentum approach (Model 1) gave slightly better agreement with their experimental observations data when using their dispersion model (PHAST).

Because the HMP and Briggs models are steady-state models, we define 11 "steady-state" time segments covering the first 100 s of the Trial 8 release. The time segments (periods) are shorter in the initial periods, when the mass emission rate is more rapidly decreasing with time. Table 1 lists the conditions determined for each time period using Expansion Model 1 and Model 2. The listed time in the first column is the end of the period (e.g., the listed time of 10 s corresponds to averaging over the time period from 5 to 10 s after release). The listed duration of release refers to the averaging time for the numbers listed in subsequent columns. The average mass flux Q_c, initial cloud temperature T_c, and mass fraction vapor apply to both Models 1 and 2. Initial cloud density (ρ_c), volume flux (V_c), vertical velocity (w_o), and radius (R_o) are outputs of both Expansion Models 1 and 2. The exit conditions used as input to Expansion Models 1 and 2 have been determined by adjusting the vapor mass fraction in the two-phase nozzle discharge model of Leung (1990) to match the time-dependent emission rate in Spicer and Tickle (2020). The measurements within the vessel show that during two-phase discharge, the pressure in the vessel is well approximated by the saturated vapor pressure. During vapor discharge, the upstream stagnation pressure is adjusted to match the observed emission rate. The vapor mass fraction at the vent exit is assumed to be the same as that inside the vessel; this amounts to a 'frozen flow' discharge

Table 1. Initial plume conditions assumed for 11 time periods after the release is initiated. The mass flux Q_c, the temperature T and the mass fraction of vapor represent conditions at the exit hole. The effective cloud density ρ_c, volume flux V_c, vertical velocity w_o and plume radius R_o represent conditions after the plume pressure decreases to ambient.

		Q_c	T_c		ρ_c	ρ_c	Q_c/ρ_c	Q_c/ρ_c	w_o	w_o	R_o	R_o
		observed	observed		Model 1	Model 2	Model 1	Model 2	Model 1	Model 2	Model 1	Model 2
Release time ending	Duration of release	Mass flux	Cloud temperature	Mass fraction vapor	Cloud density	Cloud density	Volume flux Vc	Volume flux Vc	Initial vertical velocity	Initial vertical velocity	Initial radius	Initial radius
s	s	kg/s	K		kg/m^3	kg/m^3	m^3/s	m^3/s	m/s	m/s	m	m
5	5	139.4	286.2	0.19	16.71	16.35	8.34	8.53	84.6	51.0	0.177	0.231
10	5	66.8	283.7	0.31	10.11	9.71	6.61	6.88	148.2	87.1	0.119	0.159
15	5	48.8	281.0	0.42	7.57	7.23	6.45	6.75	182.3	108.1	0.106	0.141
20	5	37.8	277.9	0.53	5.96	5.66	6.34	6.68	210.0	126.4	0.098	0.130
25	5	30.1	274.9	0.66	4.80	4.56	6.27	6.60	234.2	143.7	0.092	0.121
30	5	24.3	271.8	0.81	3.93	3.73	6.18	6.51	255.8	160.7	0.088	0.114
40	10	18.1	267.4	0.98	3.21	2.88	5.64	6.28	263.3	176.0	0.083	0.107
50	10	12.4	262.0	1	3.16	2.84	3.92	4.37	221.1	175.3	0.075	0.089
60	10	8.64	257.4	1	3.16	2.89	2.73	2.99	164.3	161.0	0.073	0.077
80	20	5.24	252.3	1	3.08	2.95	1.70	1.78	97.9	97.9	0.074	0.076
100	20	2.71	247.2	1	3.05	3.01	0.89	0.90	49.7	49.7	0.075	0.076

assumption. The advantages of applying the model of Leung (1990) are its simplicity of computation, useful when fitting to measured flow rates, together with its applicability to both the two-phase and subsequent vapor venting regimes. Reassuringly, the predicted time of transition from two-phase venting to vapor venting using the Leung (1990) discharge model agrees with the estimated transition time from visual observations.

DESCRIPTION OF DENSE GAS PLUME RISE MODELS TESTED

Three models for vertical jets of dense gases are compared with the Trial 8 observations of maximum plume rise, distance to maximum plume rise, distance to plume touchdown, and concentration at plume touchdown. The first two models (Hoot, Meroney and Peterka (HMP, 1973); and Briggs 1967) are one-line analytical formulas. The third model, DRIFT, is a comprehensive dispersion modelling program for estimating the effects of a variety of hazardous releases to the atmosphere (Tickle and Carlisle, 2013). The basic assumptions for each model are summarized below.

HMP: The Hoot, Meroney and Peterka (1973) model contains analytical one-line formulas (also see p 57 of Hanna et al. 1996) for the maximum plume rise, downwind touchdown, and concentration at touchdown, for dense gasses released vertically upwards. In the 1970s there was much concern and research about dense gases released from vents. Hoot et al. (1973) carried out wind tunnel experiments with dense plumes in cross-winds and used basic dimensional analysis principles to decide which dimensionless variables to plot and use to develop empirical relations. Extensive details and tables and plots of experimental data are in the 1973 Hoot el al. report; a briefer summary is in the conference paper by Hoot and Meroney (1974). The HMP model equations are given below.

Maximum plume rise Δh above source:

$$\Delta h/2R_o = 1.32\,(w_o/u)^{1/3}(\rho_o/\rho_a)^{1/3}[w_o^2/(2R_o g')]^{1/3} \qquad (1)$$

where $g' = g(\rho_o-\rho_a)/\rho_o$; g is acceleration of gravity (9.8 m s^{-2}), ρ_a is ambient air density, u is wind speed, and ρ_o, R_o, and w_o are initial plume density, radius and vertical velocity after depressurization.

Distance to maximum plume rise $x/2R_o = w_o u/(2R_o g')$ (2)

Plume touchdown distance x_g downwind:

$$x_g/2R_o = w_o u/(2R_o g') + 0.56\{(\Delta h/2R_o)^3\,[(2 + h_s/\Delta h)^3\text{-}1]u^3/(2R_o w_o g_a')\}^{1/2} \qquad (3)$$

where $g_a' = g(\rho_o-\rho_a)/\rho_a$ and h_s is elevation of the stack or vent opening above the ground (2 m for JR II Trial 8). Air density ρ_a is assumed to be 1.055 kg m^{-3} based upon the measured air pressure and temperature.

The HMP model also has a formula for the ratio of the maximum concentration, C_{max}, at plume touchdown to the initial concentration, C_o, after depressurization:

$$C_{max}/C_o = 2.43\ (w_o/u)\ [(h_s + 2\Delta h)/(2R_o)]^{-1.95} \quad (4)$$

where h_s is height of the source above ground (2 m for Trial 8).

Briggs: The Briggs (1969) model is based on his equation for the trajectory of a buoyant (or negatively buoyant) plume as a function of distance, x, downwind of the release point:

$$\Delta h = [(19(\rho_o/\rho_a)(M_o/u^2)x - 4.2\ (B_c/u^3)x^2]^{1/3} \quad (5)$$

where $M_o = w_o^2 R_o^2$ is proportional to the initial momentum flux and $B_c = g[(\rho_o - \rho_a)/\rho_a]w_o R_o^2$ is proportional to the initial buoyancy flux (here assumed positive for a dense cloud). The maximum rise occurs at the distance where $d(\Delta h)/dx = 0$. This equation is most often used for positively buoyant plumes, but is also valid for negatively buoyant clouds. The plume touchdown distance can be calculated as the distance where $\Delta h = 0$ (i.e., the first term in the equation equals the second term). That is, $x_g = 4.52(\rho_o/\rho_a)uM_o/B_o = 4.52\ w_o u/[g(\rho_o - \rho_a)/\rho_a]$. Briggs does not include a formula for maximum ground level concentration, C_{max}.

DRIFT: This is a commercially-available integral dispersion model that is used by HSE for its regulatory work in the UK. While DRIFT was originally conceived as a dense-gas dispersion model, it has subsequently been adapted to model dispersion of passive and buoyant sources (Tickle and Carlisle, 2008). DRIFT incorporates a momentum-jet model to simulate pressurized releases, which includes both single and two-phase jet models, where the latter assumes homogeneous equilibrium between the gas phase and the dispersed liquid droplet phase. The thermodynamic models in DRIFT are able to account for multi-component mixtures and humidity effects (condensation and evaporation of water droplets, and associated latent heat transfer), including their effect on cloud buoyancy (Tickle, 2001). Releases can be modelled at different angles to the vertical (including the vertically-upwards case in Trial 8) and also for different lateral cross-wind directions.

DRIFT assumes that the boundary layer is steady state and can be characterized by Monin-Obukhov similarity. Based on observed wind speed at 2 m, the derived roughness length (z_o = 0.5 mm) for the DPG salt playa, and a measure of upward heat flux, the model calculates the friction velocity u*, the eddy dissipation rate ε ($m^2\ s^{-3}$), and the Monin-Obukhov length L. From these inputs, a vertical profile of wind speed and turbulence is estimated. Plume dispersion is parameterized by passive entrainment terms dependent upon the eddy dissipation rate and K-theory diffusivity. A measure of lateral wind fluctuation is used to parameterize passive spreading. The dispersion of the plume is modelled as a volumetric air entrainment rate per unit length along the plume trajectory (the product of the entrainment velocity and open perimeter length of a section through the plume). For the elevated plume, the entrainment velocity is parametrized as a sum of terms representing the entrainment due to: shear as a result of

the excess velocity component along the axis of the jet, cross-flow induced entrainment associated with the component of ambient velocity perpendicular to the plume, and ambient turbulence that is proportional to the cube root of the atmospheric kinetic energy dissipation rate.

For the ground-based dense plume after touchdown, the entrainment is split into top entrainment (the product of the top entrainment velocity and plume width) and edge entrainment (the product of the edge entrainment velocity and plume height). The top entrainment velocity is proportional to the atmospheric friction velocity with a suppression factor due to stable density stratification in the dense cloud. The edge entrainment velocity includes a term dependent upon the lateral gravitational spreading velocity of the cloud and the lateral ambient velocity fluctuation, which is taken be $2u^*$. An additional lateral spread is included to represent the effect of larger scale motions resulting in lateral plume meander.

As stated earlier, DRIFT assumes steady state meteorology. However, the JR II Trial 8 release occurred in the early morning, when conditions are changing from stable to unstable. In addition, the shallow near-surface unstable layer during the Trial 8 release is capped by a deep inversion layer above about 16 or 32 m, and so the treatment within DRIFT is at best an approximation. Surface meteorological conditions during the 10 minute period after the release began have been assumed based upon the recommendations in Hanna (2020): 2.1 m/s wind speed at 2 m height, inverse Monin-Obukhov length of -0.1632 /m, surface roughness length of 0.5 mm, relative humidity of 26.5%. Despite the non-steady conditions, DRIFT's predictions of the plume trajectory are in reasonably good agreement with the observations – possibly because the trajectory is mainly affected by the mixing induced by the plume itself, rather than depending in detail upon the atmospheric turbulence.

Further details of DRIFT are discussed in Tickle and Carlisle (2013), and applications to JR II Trials 1, 6 and 7 are described in Gant et al. (2021). DRIFT Version 3.7.17 has been used for this study. The model is run "as-is" without any modifications.

Approximate account of the time-dependence of the discharge is taken by undertaking multiple runs of DRIFT's steady continuous dispersion model using release conditions corresponding to the time segments in Table 1 DRIFT predicts the centerline trajectory, which has been used to estimate the maximum height and downwind distance at which this occurs. For the touchdown point, the predicted ground-level concentration as a function of downwind distance has been examined to determine the downwind distance at which the maximum ground-level concentration occurs – this is taken to be the touchdown distance.

In addition to its steady continuous dispersion model, which neglects along-wind diffusion, DRIFT also includes dispersion models for instantaneous, finite-duration and time-varying releases which include along-wind diffusion effects. It is increasingly important to account for along-wind diffusion when considering greater downwind

distances where the cloud travel time exceeds the release duration. For the purpose of comparing concentration predictions with measurements at 85 m and beyond, DRIFT's finite-duration model has been used based upon the average release over the first 30s, corresponding approximately with the two-phase discharge region.

RESULTS

The HMP, Briggs, and DRIFT model predictions of maximum plume rise, distance to maximum plume rise, and distance to plume touchdown are compared with observations in Table 2, for assumed initial conditions at times after the release begins, t, equal to 10 and 40 s. In all cases, the models are compared for both expansion models (Model 1 and Model 2). As mentioned earlier, the observed values are estimated from videos and photos from "snapshots" at 10 s and 40 s after the release starts. However, the modeled values are assuming steady state conditions with emissions inputs from the times of 10 s and 40 s after the release starts. The HMP and Briggs models can only treat steady-state releases. The DRIFT model can treat some aspects of time-variable releases; however, it was run here in steady-state mode, to be consistent with the HMP and Briggs models.

Table 2. Comparison of observed and modeled maximum plume rise, distance x to maximum plume rise, and plume touchdown distance (all in meters) for times after release of 10 and 40 s.

	Obs	HMP Model 1	HMP Model 2	Briggs Model 1	Briggs Model 2	DRIFT Model 1	DRIFT Model 2
Maximum rise t = 10 s	40	63	45	83	59	46	31
Maximum rise t = 40 s	60	60	51	87	66	45	40
x at maximum rise t = 10 s	20	36	20	70	50	26	14
x at maximum rise t = 40 s	50	84	60	200	150	84	67
Touchdown t = 10 s	50	120	70	200	100	90	55
Touchdown t = 40 s	100	270	198	500	300	260	220

Table 2 shows that, for t = 10 s, the predicted maximum plume rise is largest for the Briggs model and smallest for the DRIFT model. There are six values of predicted maximum plume rise. Here, we define the median predicted value as the average of the 3rd and 4th ranked values. Thus, the observed maximum rise is 40 m and the median predicted maximum rise is 52 m (a 30 % overprediction). The three models' best

individual predictions of maximum rise are 45 m (about 12 % too large) for HMP Model 2, 59 m (about 50% too large) for Briggs Model 2, and 46 m (about 15% too large) for DRIFT Model 1. This agreement is good, considering all the uncertainties. For t = 40 s, the maximum plume rise predictions have about the same fractional error as for t = 10 s. The observed value is 60 m and the median of the predictions is 55 m.

Table 2 shows that, in all cases, the Model 1 expansion option produces larger plume rise predictions than the Model 2 option. The major reason for this is that (as seen in Table 1) the initial vertical velocity, w_o, is greater (by about 40 to 60 % in the first 40 s) for Model 1 than Model 2. Briggs' formula (eq. 5) indicates that, for a given volume flux, the momentum flux is larger as w_o increases. Because the distance downwind to the maximum rise and the touchdown distance will increase as maximum rise increases, those predicted distances are also larger for the Model 1 expansion option than for the Model 2 option in all cases.

The distance (x) to maximum rise is also addressed in Table 2 for the models for t = 10 s and 40 s. The observed distance was 20 m and 50 m, respectively, based on the snapshots. The median overprediction of this distance by the models was about 60 to 70 %. However, for t = 10 s, where the observed distance is 20 m, the HMP Model 2 and the DRIFT Model 2 predictions are 20 m and 14 m. The DRIFT Model 1 prediction is 26 m, which means that the two DRIFT predictions bracket the observed value of 20 m. The HMP and DRIFT Model 2 predictions are about 15 to 20 % too large for t = 40 s. The Briggs model tends to overpredict this distance by a factor of 2 to 4 for both t = 10 and 40 s.

The touchdown distance (observed to be 50 m for t = 10 s and 100 m for t = 40s) is important because that is where the maximum ground concentration is likely to be. Table 2 shows that the median model overprediction of touchdown distance is about a factor of 2 for t = 10 s and a factor of 2.6 for t = 40 s. DRIFT Model 2 is the closest for t = 10 s (observed 50 m vs predicted 55 m) and HMP Model 2 is the closest for t = 40 s (observed 100 m vs predicted 198 m). The Briggs model produced overpredictions of a factor of 2 to 5. .

It is concluded from Table 2 that the three models with the two alternate expansion models can predict maximum plume rise, distance to maximum rise, and touchdown distance within a factor of two most of the time. Often the models' predictions are within 20 or 30 % of the observations. There is no evidence whether Expansion Model 1 or 2 performs better.

Figures 4, 5, and 6 contain plots of observations and predictions of these three variables versus release time. They include the same data as Table 2, but more clearly show the trends of the different models. As discussed before, the observations listed for a certain time are based on snapshots of the plume at that time, whereas the predictions listed for that time are steady-state solutions using the mass emission rate and other initial conditions for that time after the release starts. For example, a dot at a time of 40 s for a

given model represents a steady-state calculation using inputs (from Table 1) averaged from 30 to 40 s.

Observed and predicted maximum plume rise are plotted in Figure 4 as a function of release time, t, from 0 to 100 s. Each dot represents the middle of a time period (of duration 5, 10, or 20 s) when emissions and other inputs are assumed constant. It is clearly seen that Briggs Model 1 produces the largest plume rise and DRIFT Model 2 usually produces the smallest plume rise. HMP tends to be "in the middle". The trend in maximum plume rise with time for all models is an increase with time until about 30 to 40 s, and then a decrease with time. This trend may seem counterintuitive, since the mass emission rate is continually decreasing, by a factor of about 10, over the 40 s time period. The Briggs' formula for plume rise (eq 5) can explain this. There are two terms – the first is proportional to the momentum flux, and the second is negative and proportional to the total cloud excess density. As time increases, the first term decreases in magnitude, but the second term also decreases in magnitude. Earlier, we postulated that, initially, the second term has a large effect and the cloud excess density holds the plume rise down. As time increases and approaches about 40 s the momentum flux term has more influence and the cloud excess density effect decreases. Thus, the maximum plume rise increases even though the mass flux has decreased. After about 40 s, the initial jet is "all gas" and its excess density is decreased due to the fact that imbedded chlorine aerosol drops are no longer present, so the effects of the second term diminish, and the maximum plume rise decreases as the momentum flux decreases.

The red dots in Figure 4 are the observed maximum plume rise (40 and 60 m) at times after release starts of 10 and 40 s. We can look at the figure and see that HMP Model 2 and DRIFT Model 1 produce best agreement with the observation at t = 10 s, and all six models bracket (within plus and minus about 20 to 25 m) the observation at t = 40 s.

The distance to maximum plume rise is plotted in Figure 5. The predicted trend with time follows the trend seen in Figure 4 for maximum plume rise, with a maximum at about 40 s. This is expected, since the distance to maximum plume rise is positively correlated with the maximum plume rise. As stated in the discussion of Table 2, the models tend to mostly overpredict the observed distance, especially at t = 40 s. However, the overprediction at t = 40 s is only 20 to 30 % for HMP Expansion Model 2 and DRIFT Expansion Model 2. At t = 10 s, the two DRIFT versions bracket the observation of 20 m, and HMP Expansion Model 2's prediction is 20 m.

As seen in Figure 6, the plume touchdown distances also follow the same shape as the maximum plume rise and distance to maximum rise curves. Note in Table 1 that the vapor fraction is 1.0 (i.e., the plume is all gas) after a time of 30 or 40 s. The observed distance to touchdown also increases from 50 m at t = 10 s to 100 m at t = 40 s, but all six model predictions of touchdown distance are larger than these values. Agreement is best at t = 10 s, where the DRIFT Expansion Model 2 predicts 55 m (10 % high) and the HMP Expansion Model 2 predicts 70 m (40 % high). All except the Briggs Expansion Model 1 are within about a factor of two too large for t = 10 s.

It is concluded that these models are satisfactorily capturing the basic physics and are producing predictions of maximum plume rise and distances that are usually within a factor of two of the Trial 8 observations. It is likely that better performance would be found for models that can simulate the time-variable source conditions and plume behavior, as well as account for the fact that, in the presence of wind speed shear, the elevated plume (resulting from smaller emissions after 30 or 40 s) might overtake the ground-based cloud (resulting from larger two-phase emissions in the first 10 or 20 s).

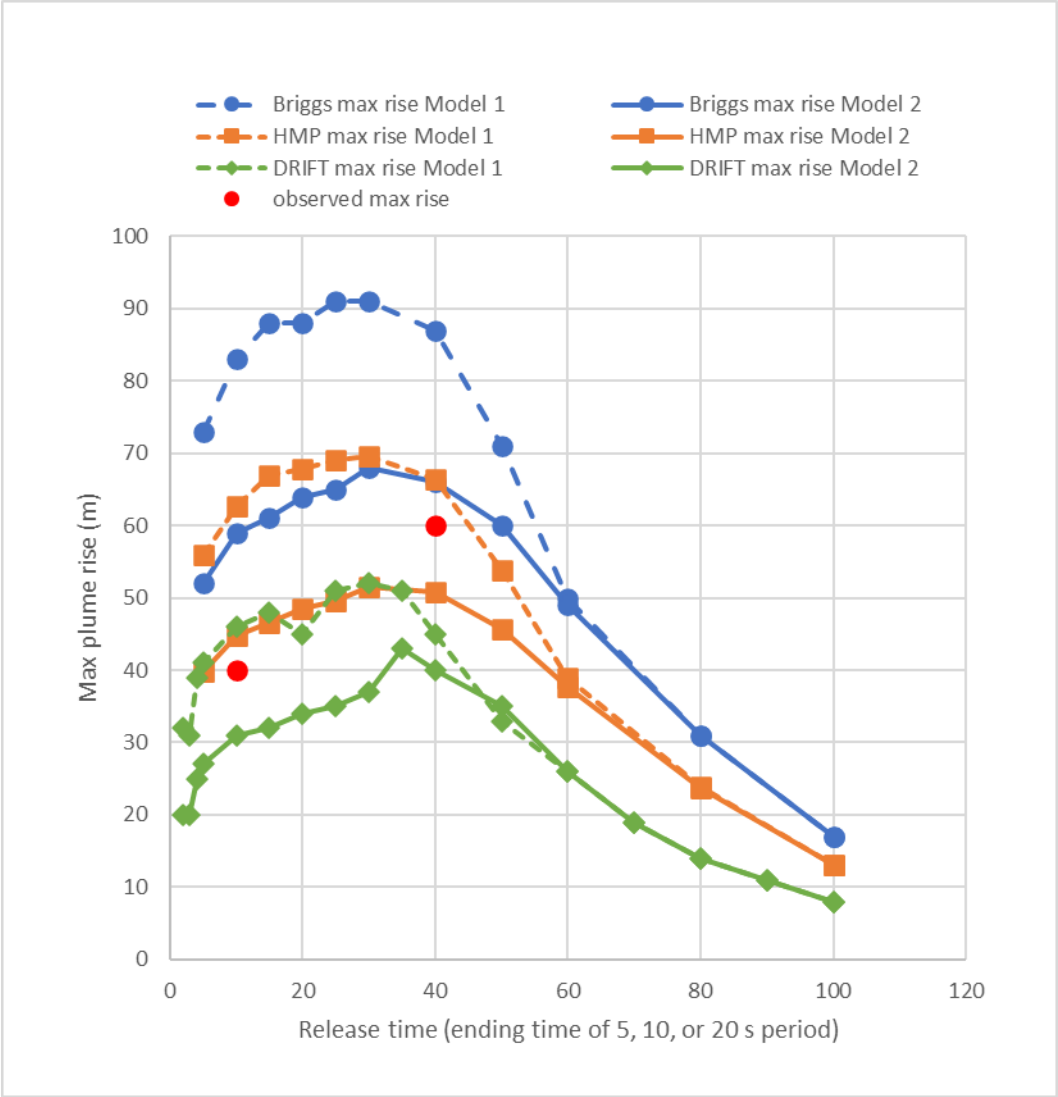

Figure 4. Observed and modeled maximum vertical plume rise, calculated using emissions rates for 11 time segments after release was initiated.

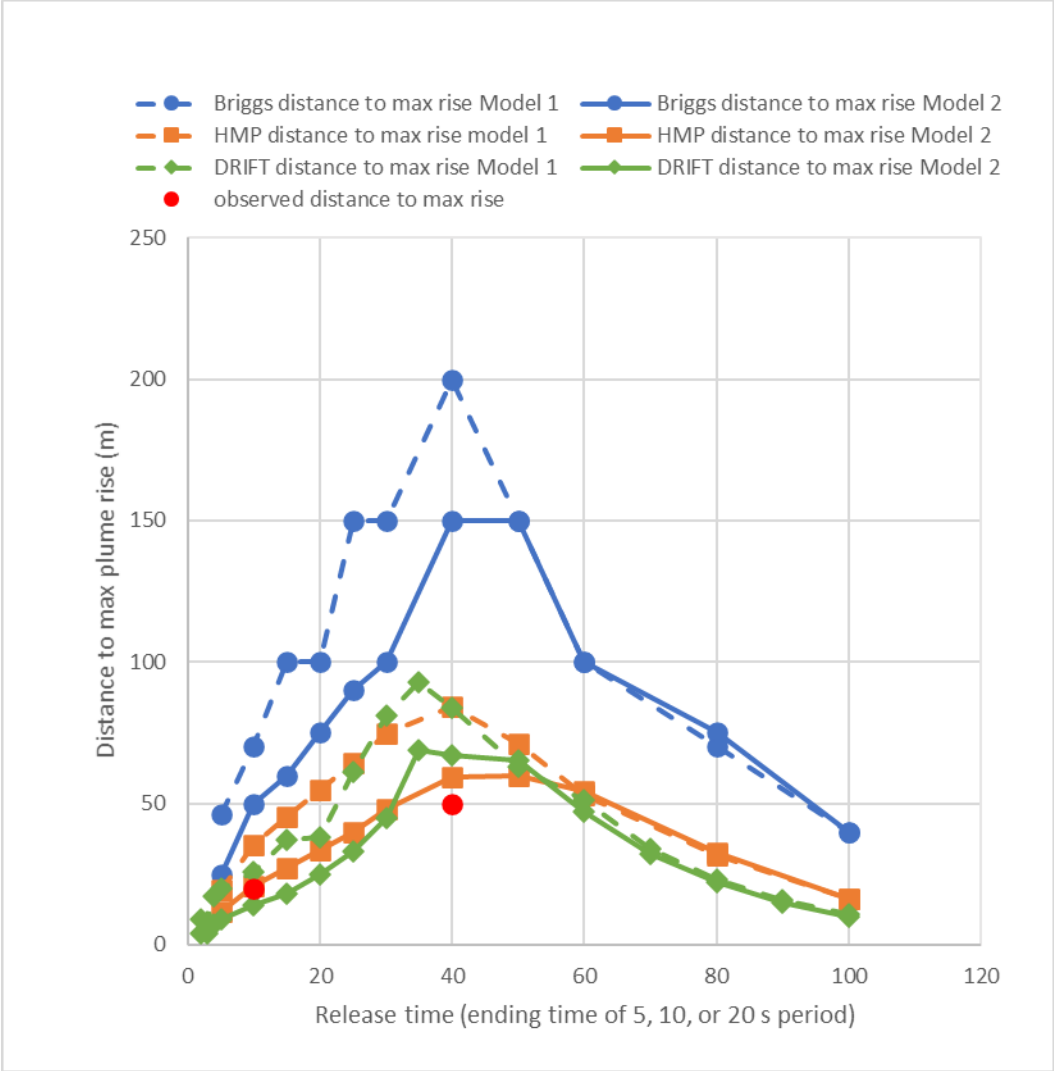

Figure 5. Observed and modeled horizontal distance to maximum plume rise, calculated using emissions rates for 11 time segments after release was initiated.

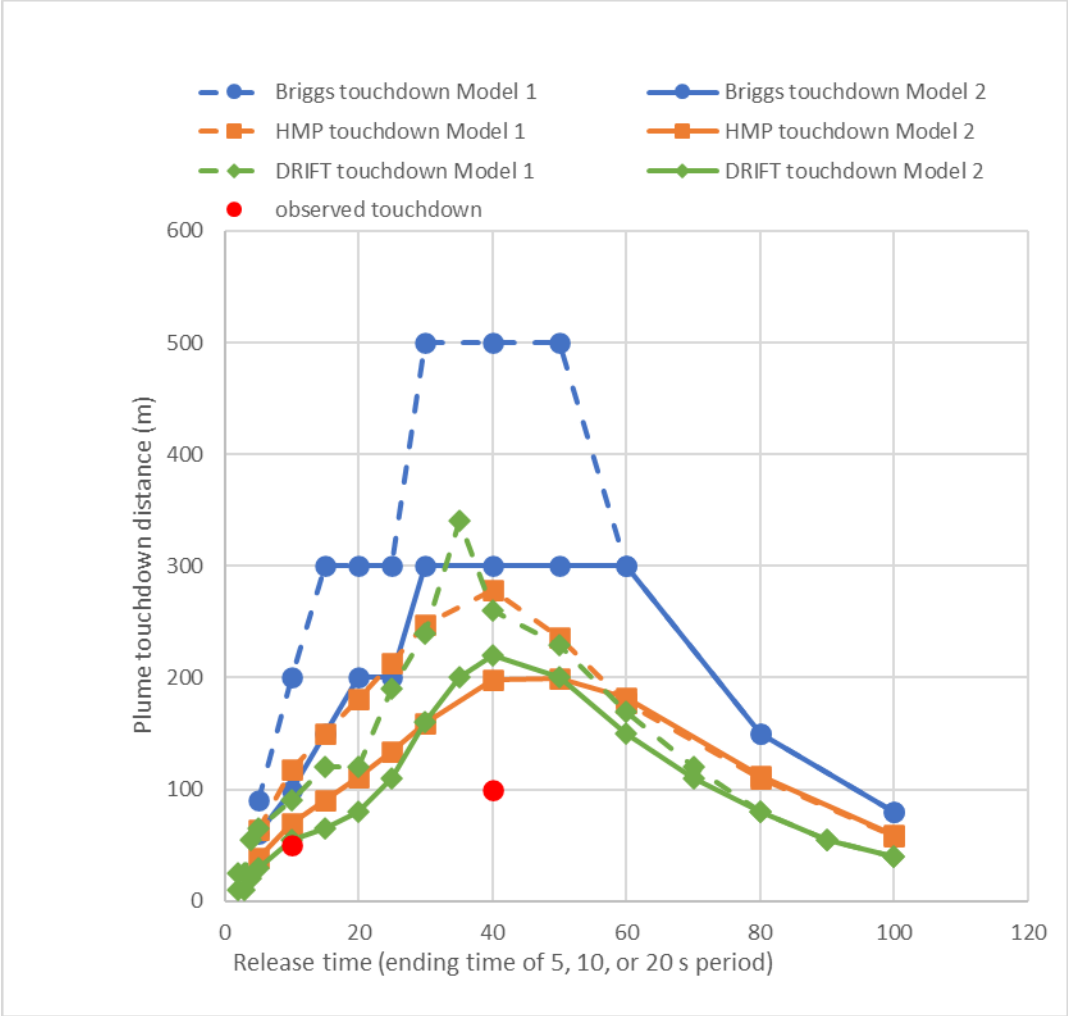

Figure 6. Observed and modeled distance to plume touchdown, calculated using emissions rates for 11 time segments after release was initiated.

The HMP and DRIFT models can also predict maximum ground-level concentrations at the location of predicted plume touchdown, which ranged from 55 to 120 m for t = 10 s and from 198 to 270 m for t = 40 s. These can be compared with the maximum observed concentration during JR II Trial 8 on the 85 m arc, which is between the observed 50 m and 100 m touchdown distances at 10 and 40 s, respectively. There were only three JAZ concentration sensors on this 85 m arc, of which two measured concentrations in excess of 10,000 ppm. The Briggs model does not predict concentrations. Table 3 lists the observed and modeled maximum concentrations. Note that the predictions for Expansion Model 2 are greater than those for Expansion Model 1, probably because the plume rise is less for Expansion Model 2 than for Expansion Model 1 for both HMP and DRIFT. The observed maximum concentration is between the Expansion Model 1 and Expansion Model 2 predicted concentrations for HMP and DRIFT. The two expansion models are alternative approximate treatments of the expansion zone that are used here to determine the input

conditions required by the models. It is interesting to see the effect of these alternative approximations on the predicted trajectory, but this is not an adjudication of correctness of either. We conclude from Table 3 that the HMP and DRIFT model predictions of maximum concentration are reasonably close to the observations (within plus and minus a factor of two).

Table 3. Comparison of observed and modeled maximum concentration. Model predictions are at touchdown distance.

	Observed at 85 m	HMP Model 1	HMP Model 2	DRIFT Model 1	DRIFT Model 2
Maximum C (ppm)	12080	9570	17660	6600	14000

Figure 7 shows a comparison of the observed and DRIFT model predicted arc-maximum concentrations at distances of 85 m and at seven additional sampling arcs extending to 11 km. The observations are all made at a sensor height of 0.3 m. In addition, the HMP model predictions (listed in Table 3) are shown at predicted plume touchdown distance. The observed values are from Chang et al. (2021). The DRIFT predictions with Expansion Model 2 are seen to have relatively small mean bias out to 2 km, while the DRIFT predictions with Expansion Model 1 are biased about a factor of two low, on average. The observations at the 5 and 11 km arcs are very small, less than 1 ppm, due to the cloud passing off the edge of the sampling arcs.

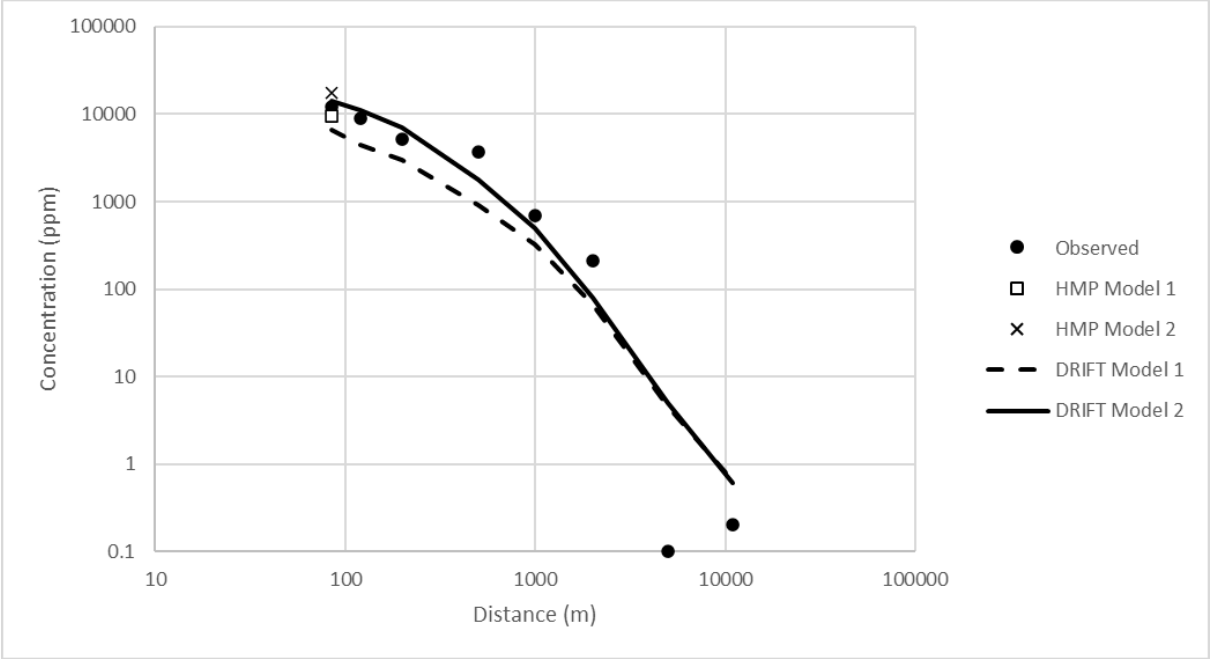

Figure 7. Arc-maximum observed and predicted concentration as a function of distance. Observations are made at z = 0.3 m.. DRIFT centerline (arc-maximum) predictions are made for the sensor height. The figure also contains the HMP model predictions at plume touchdown.

CONCLUSIONS

JRII Trial 8 is a unique one-of-a-kind field experiment that provides useful insight into the behavior of vertically-upwards releases of pressure-liquefied chlorine from large holes in large storage vessels. Despite the hole being located on the top of the tank, i.e. in the vapor space, the release rapidly transitioned within the first few seconds from gaseous to two-phase, due to liquid swell pushing the boiling liquid out of the vessel. After expansion, the resulting two-phase plume has an effective density of about 12 (five times larger than that of chlorine gas alone), due to the presence of tiny aerosols with median diameters of about 50 μm (Britter et al, 2011). The very dense chlorine plume first rises up due to its momentum and then bends over and sinks towards the ground.

Video footage and still photographs from Trial 8 were used to examine the trajectory of the dense jet, focusing on the horizontal and vertical distances reached by the plume at different times. Distances on the photos were scaled using the known height of a camera tower near the source, and are thought to be accurate within about 20 %. During the first 10 seconds of the release, the videos showed the dense jet rising to a height of around 40 m, then sinking to the ground and touching down at a horizontal distance from the tank of about 50 m. The plume then hit the ground and spread out radially in all directions to a distance of about 30 or 40 m due to gravity slumping. Over time, the pressure in the vessel decreased, the boiling liquid level decreased below the orifice and the jet transitioned from two-phase to gaseous. Due to the reduction in density of the jet, the chlorine vapor discharged from the vessel remained aloft at later times (greater than about 30 or 40 s) and dispersed as an elevated plume, without sinking towards the ground. Meanwhile, the dense cloud that touched down in the early phase of the release continued to move downwind along the ground as a typical "pancake-shaped" dense gas cloud.

The predictions of three integral models were compared to the observed initial dense jet plume rise and touchdown distance: 1) the analytical formulas suggested in 1973 by Hoot, Meroney, and Peterka (HMP), 2) the Briggs (1969) analytical formula for plume trajectory, and 3) the DRIFT dispersion software (Tickle and Carlisle, 2013). All three models were shown to usually agree with the observed distances within about a factor of two. The Briggs model predictions of the distance to maximum plume rise and touchdown were about a factor of two to five too large. Additionally, the HMP and DRIFT models predicted chlorine concentrations near the plume touchdown position within a factor of two of the observations.

The work presented here demonstrates that integral dispersion models are able to predict the correct physical behavior for vertically-upwards directed dense jets if they are provided with suitable inputs, in terms of the discharge conditions from the orifice. The Briggs formula for plume rise provides useful insight into the physical behavior of a dense plume, namely the competition between momentum and buoyancy forces.

The other experiments in the JR II series (Trials 1-7 and 9) involved releases from the liquid space in base of the tank or a 45-degree downwards position, and they all resulted in much higher downwind concentrations than in Trial 8 (Chang et al., 2021). In emergency response or risk assessment scenarios where the release location is unknown, releases from the underside of a vessel can provide conservative estimates for the ground-level downwind concentrations. Nevertheless, there are cases where releases from the vapor space needs to be assessed. The work presented here provides useful information to help examine those scenarios.

There are several caveats to our conclusions that concern the uncertainties in the analysis. The releases were complex, involving changes over time of phase, composition, release rate, temperature, and velocity. Our method of estimation of distances using photos has inherent uncertainties of about 20 %. Nevertheless, there is merit in comparing with measurements made from video and still images. The measurements show clear trends in the evolution of the plume trajectory which are largely matched by the model predictions. Agreement of the three models' (HMP, Briggs, and DRIFT) predictions with the observations is within margins which are generally recognized as being adequate for acceptability within the realms of major hazard consequence modelling.

ACKNOWLEDGEMENTS – Steven Hanna and Thomas Mazzola's research has been sponsored primarily by the U.S. Defense Threat Reduction Agency (DTRA). Graham Tickle and Simon Gant's contributions were funded by the UK Health and Safety Executive. The contents of the paper, including any opinions and/or conclusions expressed or recommendations made, are those of the authors alone and do not necessarily reflect HSE policy.

REFERENCES

Allason, D, K. Armstrong, J. Barnett, P. Cleaver, and A. Halford, 2014: Behaviour of releases of carbon dioxide from pipelines and vents. Proc. 10th Int. Pipeline Conf IPC2014. ASME, IPC2014-33384, 10 pp.

Bauer, T.J., 2013: Comparison of chlorine and ammonia concentration field trial data with calculated results from a Gaussian atmospheric transport and dispersion model. J. Haz. Mat. 254-255, 325-335.

Bodurtha, F., 1961: The behavior of dense stack gases. J. Air Poll. Control Assoc., 11, 431-437.

Briggs, G.A., 1969: Plume Rise. AEC Critical review Series, Div. of Tech. Inf., TID-25075.

Britter, R, J. Weil, J. Leung, and S. Hanna, 2011: Toxic industrial chemical (TIC) source emissions modelling for pressure liquefied gases, Atmos. Environ. Vol 45, 1-25, doi:10.1.1016/j.atmosenv.2010.09.021

Chang, J., T. Mazzola, and S. Hanna, 2021: Analysis of Observed Concentrations from the Jack Rabbit II Sampler Network for Use in Evaluating Dispersion Models. Atmos. Environ. 246. https://doi.org/10.1016/j.atmosenv.2020.117997.

Cleaver, R.P, and Edwards, P.D., 1990: Comparison of an integral model or predicting the dispersion of a turbulent jet in a cross-flow with experimental data. J. Loss Prev. Process Ind. 3, 91-96.

Ewan, B., and K. Moodie, 1986: Structure and velocity measurements in underexpanded jets, Combust. Sci. and Tech. Vol. 45, 275-288

Fox, S., S. Hanna, T. Mazzola, T. Spicer, J. Chang, and S. Gant, 2021: Overview of Jack Rabbit II (JR II) field experiment and summary of the methods used in the dispersion model comparison. To appear in Atmos. Environ.

Fox, S. and D. P. Storwold, 2011: Project Jack Rabbit Field Tests. Chemical Security and Analysis Center, Science and Technology Directorate, US Dept. of Homeland Security, CSAC 11-006,USA, 162 pp.

Gant, S., G. Tickle, A. Kelsey, and H. Tucker, 2021: DRIFT dispersion model predictions for the Jack Rabbit II model inter-comparison exercise", Atmos. Environ. Vol. 244, 1 Jan 2021, 117717, https://doi.org/10.1016/j.atmosenv.2020.117717

Hanna, S.R., 2020: Meteorological data recommendations for input to dispersion models applied to Jack Rabbit II trials. Atmos. Environ. 235, 16 pp. https://doi.org/10.1016/j.atmosenv.2020.117516

Hanna, S.R., R.E. Britter, J. Chang and E. Argenta, 2012: The Jack Rabbit chlorine release experiments: Implications of dense gas removal from a depression and downwind concentrations. J. Haz. Mat., **213-214**, 406-412.

Hanna, S.R., J. Chang and P. Huq, 2016: Observed chlorine concentrations during Jack Rabbit I and Lyme Bay field experiments. Atm. Environ., **125**, 252-256.

Hanna, S.R., P.J. Drivas and J.C. Chang, 1996: Section 5.2.1 Momentum-dominated jets, and 5.2.2 Elevated dense gas jets (pp 52-58). Guidelines for Use of Vapor Cloud Dispersion Models. AIChE/CCPS, 345 East 47th St., New York, NY, USA, 285 pp + CD.

Hoot, T. and R. Meroney, 1974: The behavior of negatively buoyant stack gases. CEP73-74RNM-TGH33, Presented at 67th Ann. Mtg. of the Air Pollution Control Association, Denver, 21 pp.

Hoot, T., R. Meroney and J. Peterka, 1973: Wind tunnel tests of negatively buoyant plumes. EPA 650/3-74-003, USA, 108 pp.

Leung, J.C., 1990: Two-phase discharges in nozzles and pipes – a unified approach, J. Loss Prev. Process Ind. Vol. 37, Jan 1990, 27-32

Mazzola T., et al., 2021. Results of comparisons of predictions of 17 dense gas dispersion models with observation from the Jack Rabbit II chlorine field experiment", Atmos. Env. Vol. 244, 1 Jan 2021, 117887, https://doi.org/10.1016/j.atmosenv.2020.117887 .

Nicholson, D., A. Hedrick, N. Lian and E. Schmidt, 2017: Final Test Report for Jack Rabbit (JR) II. WDTC-SPD-FTR-001, US Army Dugway Proving Ground, Dugway, UT, USA, 120 pp.

Ooms, G. and N. Duijm, 1984: Dispersion of a stack plume heavier than air. IUTAM Symposium on atmospheric dispersion of heavy gases and small particles. 23 pp.

Ooms, G, A. Mathieu and F. Zelis, 1974: The plume path of vent gases heavier than air. Loss Prevention and Safety Promotion. 1, 211-215.

924 Ponsardin, P., 2017: Final Test Report: REVEAL Data Analysis Results from 2016
925 Jack Rabbit II Field Testing, Defense Threat Reduction Agency Report DTRA
926 FTR-17-03, Jan 25, 2017
927 Schatzmann, M., W. Snyder, and R. Lawson, 1995a: Building effects on dense jet
928 dispersion. CCPS Annual International Conference and Workshop on Modeling
929 and Mitigation the Consequences of Accidental Releases of Hazardous Materials,
930 p359-378, https://www.aiche.org/academy/conferences/international-conference-
931 and-workshop-on-modeling-and-mitigation-consequences-accidental-
932 releases/1995/proceeding/session/technical-papers.
933 Schatzmann, M., W. Snyder, and R. Lawson, 1995b: Experiments with heavy gas jets
934 in laminar and turbulent cross-flows. Atmos. Environ, 27A, 1105-1116.
935 Spicer,T., and D. Miller 2018: Quantifying the mass discharge rate of flashing two-
936 phase releases through simple holes to the atmosphere, Process Saf. Prog. 37,
937 382-396
938 Spicer, T. and G. Tickle, 2020: Simplified source description for atmospheric dispersion
939 model comparison of the JR II chlorine field experiments. Atmos. Environ. 244.
940 https://doi.org/10.1016/j.atmosenv.2020.117866
941 Tickle, G.A., 2001, Thermodynamic Modelling of Anhydrous HF / Moist Air /
942 Immiscible Component Mixtures and Validation against Experimental Data, AEA
943 Technology Report AEAT/NOIL/27328006/002 (R) Issue 2, June 2001.
944 Tickle, G.A. and J.E. Carlisle, 2008: Extension of the dense gas dispersion model DRIFT
945 to include buoyant lift-off and buoyant rise, Research Report RR629, Health and
946 Safety Executive, http://www.hse.gov.uk/research/rrhtm/rr629.htm
947 Tickle, G.A. and J.E. Carlisle, 2013: DRIFT Version 3.6.7: Mathematical Model
948 Description, ESR Technology Ltd, Birchwood Park, Warrington, UK, 19 Dec
949 2013.
950 Turner, J.S., 1966: Plumes with negative or reversing buoyancy. J. Fluid Mech., 26, 779-
951 792.
952 Witlox, H.W.M., M. Fernandez, M. Harper, and J. Stene, 2017: Modelling and validation
953 of atmospheric expansion and near-field dispersion for pressurised vapour or two-
954 phase releases, J. Loss Prev. Proc. Ind., 48, 331-344,
955 http://dx.doi.org/10.1016/j.jlp.2017.05.005.
956 Xiao-Yun, L., H. Leijdens, and G. Ooms, 1985: An experimental verification of a
957 theoretical model for the dispersion of a stack plume heavier than air. Atmos.
958 Environ., 6, 1087-1094.